New Physics: Sae Mulli,
Vol. 68, No. 1, January 2018, pp. 55∼61
http://dx.doi.org/10.3938/NPSM.68.55

Phase Shift Analysis and the Optical Potential Obtained by Using Inversion for α + ^{58}Ni Elastic Scattering

Yong Joo Kim*
Department of Physics and Research Institute for Basic Sciences, Jeju National University, Jeju 63243, Korea

Seok Jae Lee
Department of Biomedical Engineering, Seonam University, Namwon 55724, Korea

(Received 8 September 2017 : revised 8 October 2017 : accepted 10 November 2017)

The data for the elastic scattering of 288, 340, and 386 MeV alpha particles on ^{58}Ni was analyzed using the McIntyre parametrization for the phase shift. The calculated differential cross sections for the α + ^{58}Ni system fit the experimental data fairly well. The diffractive oscillatory structures observed in the angular distributions were explained as being due to the strong interference between the near-side and the far-side scattering amplitudes. The corresponding optical potentials were predicted by using the inversion procedure of the McIntyre phase shift. The inversion potentials were then compared with the available ones obtained from optical model analyses.

PACS numbers: 25.70.-z, 25.55.Ci, 24.10.Ht
Keywords: Phase shift analysis, McIntyre parametrization, Optical potential by inversion, Elastic scattering, α + ^{58}Ni

I. INTRODUCTION

One of the measuring quantities in the elastic scattering between heavy-ions is the differential cross section. The important element in describing the elastic differential cross section is the nuclear phase shift. Since this nuclear phase shift can be expressed as a parametrized form, the parametrized phase shift model has been used as a convenient tool in interpreting the elastic scattering data. Until now, several forms for parametrized phase shift model are known [1]. There has been a great deal of efforts [2–7] in describing the heavy-ion elastic scattering within the framework of parametrized phase shift model. For instance, the elastic data of 1503 MeV ^{16}O scatterings on ^{12}C, ^{40}Ca, ^{90}Zr, and ^{208}Pb target nuclei and ^{12}C + ^{12}C system at 360 and 1016 MeV have been analyzed [2] successfully by using phase shift based on McIntyre parametrization [8]. Further, a systematic study of elastic scattering for the ^{12}C + ^{12}C system in the range E_{lab} = 240 to 2400 MeV has been done [6] with the parametrized phase shift model.

In addition to the differential cross section, optical potential is one of the central subjects in the study of heavy-ion elastic scattering. The connection between the optical potential and elastic data (primarily differential cross section) is the nuclear phase shift. The parameters of nuclear phase shift are employed to determine the optical potential by solving the inverse scattering problem. Several attempts [9–14] have been made to evaluate the optical potential from the parametrized phase shift. By solving the inversion problem at high energies, Fayyad *et al.* [9] related the parameters of McIntyre phase shift to the ones of Woods-Saxon type optical potential. The inversion potentials [14] for the ^{12}C + ^{12}C system in the range E_{lab} = 240 to 2400 MeV were obtained, and compared with other works.

In our earlier paper [15], we reported a phase shift analysis based on the McIntyre parametrization for ^{12}C + ^{90}Zr and ^{12}C + ^{208}Pb elastic scatterings at E_{lab} = 35 MeV per nucleon. Using a phase shift analysis based on McIntyre parametrization of $S-$matrix, we analyzed

*E-mail: yjkim@jejunu.ac.kr

the ^{16}O + ^{28}Si elastic scattering at E_{lab} = 1503 MeV, calculated the optical potential by inversion, and discussed the first-order eikonal correction effect on this inversion potential [16]. Recently, the elastic scattering of the α particles on ^{16}O, ^{24}Mg, ^{28}Si, ^{58}Ni, ^{116}Sn, and ^{197}Au targets at E_{lab} = 240 MeV have been analyzed [17] by using the parametrized phase shift model. In this paper, we present a phase shift analysis based on McIntyre parametrization for the α + ^{58}Ni elastic scattering at E_{lab} = 288, 340, and 386 MeV, respectively. The parameter values of McIntyre phase shift obtained from fitting the elastic data are used for extracting the optical potential by inversion. Then, the inversion potentials are compared with the available optical model ones. In the following section, we recall the expression of the McIntyre phase shift. The formalism related with the inversion potential is briefly presented in Sec. III. Section IV is devoted to the results and discussion, in which we perform a phase shift analysis of α + ^{58}Ni elastic scattering and calculate optical potential by inversion. Finally, we provide the concluding remarks in Sec. V.

II. MCINTYRE PARAMETRIZATION FOR NUCLEAR PHASE SHIFT

The elastic scattering amplitude for spin-zero charged particle from a target nucleus may be written as

$$f(\theta) = f_R(\theta) + \frac{1}{ik}\sum_{L=0}^{\infty}(L+\frac{1}{2})\exp(2i\sigma_L)(S_L-1)P_L(\cos\theta), \quad (1)$$

where $f_R(\theta)$ is the usual Rutherford scattering amplitude, k is the wave number and σ_L denotes the Coulomb phase shift. The nuclear S-matrix element, S_L, is related to the nuclear phase shift $\chi(L)$ through the relation

$$S_L = \exp[i\chi(L)] = \exp[i\{\chi_R(L) + i\chi_I(L)\}]. \quad (2)$$

In the McIntyre parametrization [8] for nuclear phase shift, the real and imaginary parts of $\chi(L)$ are expressed as

$$\chi_R(L) = 2\mu\left[1+\exp(\frac{L-L'_g}{\Delta'_g})\right]^{-1} \quad (3)$$

and

$$\chi_I(L) = \ln\left[1+\exp(\frac{L_g-L}{\Delta_g})\right]. \quad (4)$$

The reduced radius $r_{1/2}$ and the diffusivity d_s are related with the grazing angular momentum L_g and the angular momentum width Δ_g through the following semiclassical relationship [2]:

$$L_g = kR_{1/2}(1-\frac{2\eta}{kR_{1/2}})^{1/2} \quad (5)$$

and

$$\Delta_g = kd_s(1-\frac{\eta}{kR_{1/2}})(1-\frac{2\eta}{kR_{1/2}})^{-1/2}, \quad (6)$$

where $R_{1/2} = r_{1/2}(A_P^{1/3} + A_T^{1/3})$ and η the Sommerfeld parameter. Similarly, the grazing angular momentum L'_g and its width Δ'_g in Eq. (3) can be obtained from the phase radius r_{ph} and the phase diffusivity d_{ph} instead of $r_{1/2}$ and d_s in Eqs. (5) and (6).

By using the relations $kb = L + 1/2$, $kb_0 = L_g + 1/2$, $kb'_0 = L'_g + 1/2$, $d = \Delta_g/k$, and $d' = \Delta'_g/k$, the nuclear phase shift given in Eqs. (3) and (4) can also be written in terms of impact parameters b, b_0, and b'_0:

$$\chi_R(b) = \frac{2\mu}{1+\exp[(b-b'_0)/d']} \quad (7)$$

and

$$\chi_I(b) = \ln[1+\exp(\frac{b_0-b}{d})]. \quad (8)$$

III. OPTICAL POTENTIAL BY INVERSION

The inversion solution to Woods-Saxon type optical model potential $U_{op}(r) = V(r) + iW(r)$ determined from the McIntyre parametrization of the $S-$matrix was reported by Fayyad *et al.* [9]. The obtained results are

$$V(r) = -\frac{V_0}{1+\exp[(r-R')/\Delta']} \quad (9)$$

and

$$W(r) = -\frac{W_0}{1+\exp[(r-R)/\Delta]}, \quad (10)$$

where V_0 and W_0 denote the depths of the optical model potential given by [9]

$$V_0 = \frac{4\mu E}{\pi k\alpha} \quad (11)$$

Table 1. Input parameters and χ^2/N values in the McIntyre phase shift analysis for the α + ^{58}Ni elastic scatterings at E_{lab} = 288, 340, and 386 MeV, respectively.

E_{lab} (MeV)	L_g	Δ_g	L'_g	Δ'_g	μ	χ^2/N^a
288	41.9360	4.2031	31.8862	6.2956	4.277	5.98
340	45.9064	5.3589	32.9280	7.1266	4.086	1.87
386	48.8616	5.7097	33.9365	7.7135	4.073	2.01

[a] 10% error bars, $\chi^2/N = (1/N)\sum_{i=1}^{N}\left[\frac{\sigma_{\rm th}(\theta_i)-\sigma_{\rm ex}(\theta_i)}{\Delta\sigma_{\rm ex}(\theta_i)}\right]^2$

and

$$W_0 = \frac{2E}{\pi k\beta} \tag{12}$$

with

$$\alpha = \frac{2}{\pi}\cdot[1+\exp(-\frac{b'_0}{d'})]I_0(R',\Delta'), \tag{13}$$

$$\beta = \frac{2}{\pi}\cdot\frac{I_0(R,\Delta)}{\ln[1+\exp(b_0/d)]}. \tag{14}$$

In Eq. (13), $I_0(R',\Delta')$ is given by

$$I_0(R',\Delta') = R' + \Delta'\ln[1+\exp(-\frac{R'}{\Delta'})] \tag{15}$$

and $I_0(R,\Delta)$ in Eq. (14) is obtained in a similar manner in terms of R and Δ. The remaining four potential parameters R', Δ', R, and Δ are obtained by solving the following two sets of nonlinear simultaneous equations of Ref. [9]. For the parameters (R' and Δ') related with the real potential

$$\frac{I_4(R',\Delta')}{I_2(R',\Delta')} = \frac{3}{2}\frac{I_3(b'_0,d')}{I_1(b'_0,d')} \tag{16}$$

and

$$\frac{I_6(R',\Delta')}{I_4(R',\Delta')} = \frac{5}{4}\frac{I_5(b'_0,d')}{I_3(b'_0,d')}. \tag{17}$$

For the parameters (R and Δ) related with the imaginary potential

$$\frac{I_4(R,\Delta)}{I_2(R,\Delta)} = \frac{3}{4}\frac{I_4(b_0,d)}{I_2(b_0,d)} \tag{18}$$

and

$$\frac{I_6(R,\Delta)}{I_4(R,\Delta)} = \frac{5}{6}\frac{I_6(b_0,d)}{I_4(b_0,d)}, \tag{19}$$

where $I_\nu(x_0,a_0)$ is an integral given by

$$I_\nu(x_0,a_0) = \int_0^\infty \frac{x^\nu}{1+\exp[(x-x_0)/a_0]}dx \tag{20}$$

which can be evaluated analytically [18].

IV. RESULTS AND DISCUSSION

Following the approach outlined in Sec. II, we have calculated the elastic differential cross sections of α + ^{58}Ni system at E_{lab} = 288, 340, and 386 MeV by using the phase shift based on McIntyre parametrization. The five input parameters (L_g, L'_g, Δ_g, Δ'_g, and μ) are obtained from the χ^2-fit and are listed in Table 1, together with the χ^2/N values. The characteristics appearing in this Table are: (1) the grazing angular momentum L'_g for the real phase shift is smaller than the one L_g for the imaginary phase shift, (2) the two grazing angular momentum $L'_g s$ and the corresponding widths $\Delta'_g s$ increase as the incident energy increases. The calculated elastic angular distributions are presented in Fig. 1 together with the experimental data [19,20]. In this figure, the solid curves and solid circles with error bars denote the calculated results and the experimental data, respectively. Our calculations reproduced satisfactorily the diffractive oscillatory structures appearing on the angular distributions, and showed fairly good agreement with the experimental data over the whole angular range, though there exists some mismatches around 10° ∼ 20° for E_{lab} = 288 MeV. We can see that the phase shift based on McIntyre parametrization works well in the description of α + ^{58}Ni elastic scatterings at 288, 340, and 386 MeV, respectively.

The near-side and the far-side decompositions of the elastic scattering amplitude [21] have been carried out to understand the nature of elastic cross sections. The contributions of the near-side (dotted curves) and the far-side (dashed curves) components to the elastic scattering cross sections are shown in Fig. 2 along with the differential cross sections (solid curves). This figure shows that a near-side contribution dominates at small angles and a far-side one at large angles. The differential cross section

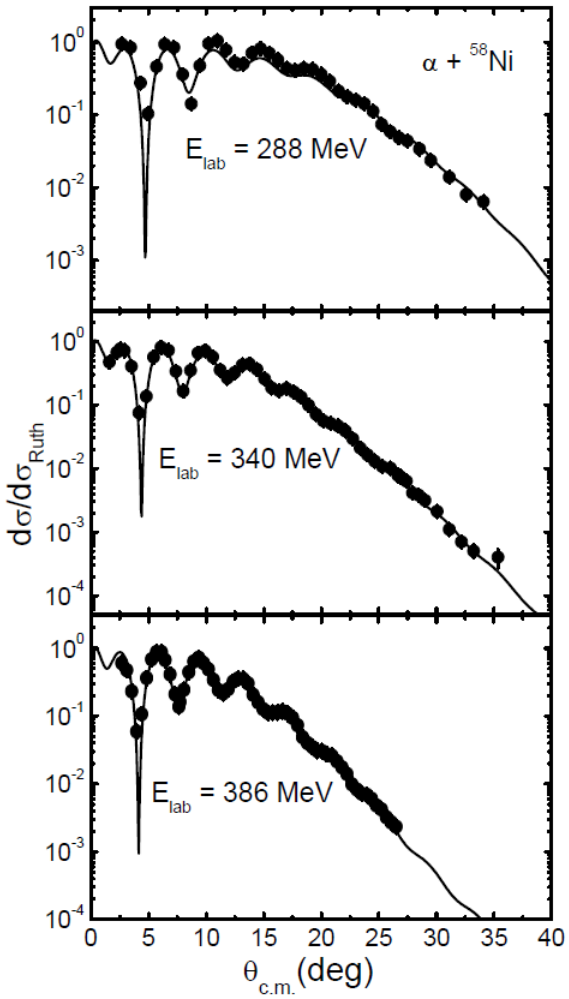

Fig. 1. Elastic scattering angular distributions for the α + ^{58}Ni system at 288, 340, and 386 MeV, respectively. The solid circles denote the experimental data taken from Ref. [19] (for E_{lab} = 288 and 340 MeV) and Ref. [20] (for E_{lab} = 386 MeV). The solid curves are the calculated results from McIntyre phase shift.

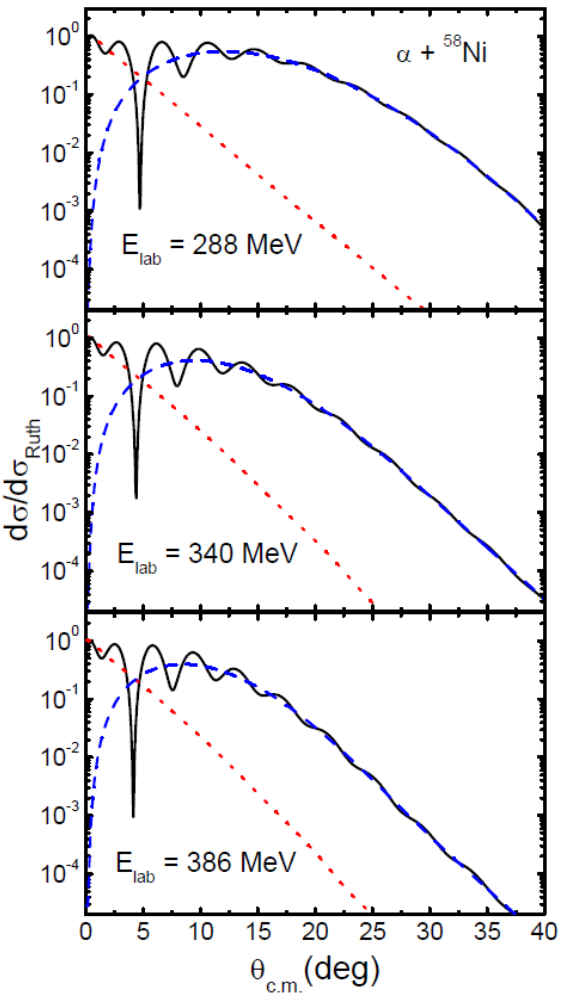

Fig. 2. (Color online) Differential cross sections (solid curves), near-side contributions (dotted curves) and far-side contributions (dashed curves) following the Fuller's formalism [21] by using the McIntyre phase shift for the α + ^{58}Ni elastic scatterings at 288, 340, and 386 MeV, respectively.

is not just a sum of the near-side and the far-side cross sections, but contains an interference between the near-side and the far-side amplitudes. The diffractive oscillatory structures observed in the elastic cross sections are considered to be due to the strong interference between the near-side and the far-side components. As Fig. 2 and Table 2 show, the near-side and the far-side contributions have a same magnitude at the crossing angles θ_{cross} = 4.90°, 4.60°, and 4.30° for E_{lab} = 288, 340, and 386 MeV, respectively, indicating that θ_{cross} is found to decrease as the incident energy increases. However, the far-side cross sections become important as the scattering angle increases from θ_{cross}. The structureless exponential fall-off behaviors of the large-angle cross sections are mainly determined by the far-side amplitude.

The results of phase shift analysis based on McIntyre parametrization are collected in Table 2. In this Table, $\theta_{n.r.}$ is the nuclear rainbow angle corresponding to minimum in the deflection function given by the formula $\theta_L = (d/dL)[2\sigma_L + \chi_R(L)]$. The nuclear rainbow angles are -15.73°, -13.10°, and -12.10° for α + ^{58}Ni system at E_{lab} = 288, 340, and 386 MeV, respectively, indicating that nuclear rainbow is clearly presented. The $L_{1/2}$ is the critical angular momentum corresponding to $|\exp(-\chi_I(L_{1/2}))|^2 = 1/2$, and is found to show an increase as the incident energy increases. The critical

Table 2. Results of McIntyre phase shift analysis for the $\alpha + {}^{58}$Ni elastic scatterings at $E_{lab} = 288$, 340, and 386 MeV, respectively.

E_{lab} (MeV)	$r_{1/2}$ (fm)	d_s (fm)	r_{ph} (fm)	d_{ph} (fm)	θ_{cross} (deg)	$\theta_{n.r.}$ (deg)	$L_{1/2}$	R_s (fm)	σ_{R_s} (mb)	σ_R (mb)
288	1.134	0.605	0.869	0.906	4.90	-15.73	45.64	6.79	1450	1443
340	1.138	0.710	0.823	0.944	4.60	-13.10	50.63	6.90	1497	1515
386	1.134	0.710	0.794	0.959	4.30	-12.10	53.89	6.88	1486	1510

Table 3. Optical potential parameter values obtained from the inversion method for the $\alpha + {}^{58}$Ni elastic scatterings at $E_{lab} = 288$, 340, and 386 MeV, respectively.

E_{lab} (MeV)	$R'(fm)$	$\Delta'(fm)$	$R(fm)$	$\Delta(fm)$	$V_0(MeV)$	$W_0(MeV)$
288	5.27073	0.833804	4.72171	0.722836	62.5745	82.9313
340	4.9819	0.876459	4.71911	0.801828	68.4693	77.3103
386	4.80287	0.893549	4.71061	0.801356	75.2393	82.3846

angular momentum has an influence on the strong absorption radius R_s. The R_s is defined as the distance of closest approach determined from the formula $R_s = \{\eta + \sqrt{\eta^2 + L_{1/2}(L_{1/2}+1)}\}/k$, and also reflected in the reaction cross section. Table 2 shows, the geometrical reaction cross sections ($\sigma_{R_s} = \pi R_s^2$) are comparable to the ones (σ_R) obtained from partial wave sum.

We have calculated the optical potential through the inversion procedure mentioned in Sec. III. Using the parameters (L_g,L'_g, Δ_g, Δ'_g, and μ) of McIntyre parametrization for phase shift, we obtained the impact parameters (b_0 and b'_0) and the diffusivity quantities (d and d'). Note that Coulomb effects were not taken into account in evaluating the parameters cited above. The inversion potential parameters (R, Δ, R', and Δ') were calculated from Eqs. (16)-(19), which can be solved by an iteration procedure such as Newton Method. The parameters α and β needed for evaluating the potential depths are determined from Eqs. (13) and (14). Finally, the inversion potential depths (V_0 and W_0) are directly obtained from Eqs. (11) and (12). The parameter values of inversion potential are given in Table 3.

The calculated inversion potentials are displayed by the solid curves in Figs. 3 and 4. Meanwhile, the dotted, dashed-dotted and dashed curves in these figures are the Woods-Saxon optical potentials obtained with the parameter Set 1, Set 2, and Set 3 of Table 2 in Ref. [19]. In the case of $E_{lab} = 386$ MeV, we presented only the inversion potential because the Woods-Saxon optical potential was not available. As a whole, the inversion optical potentials agree with the ones from the optical model analysis [19] in the surface region around the strong absorption radius. We found that the real potentials obtained from inversion procedure provide better agreements with the Woods-Saxon type optical potentials from optical model analysis [19] than the imaginary ones. From Figs. 3 and 4, it is seen that both the real and imaginary parts of the inversion potential differ greatly from those of the Woods-Saxon optical potentials in the interior region. Of course, the dotted, dashed-dotted and dashed curves were shown to be different in small r regions. Such large disagreements between four curves are hardly surprising. Since the elastic scattering data are sensitive mainly to the surface region, somewhat big discrepancies at small r regions between optical potentials from the inversion method and optical model are of little significance.

V. CONCLUDING REMARKS

In this paper, we have studied the elastic scattering of $\alpha + {}^{58}$Ni system at $E_{lab} = 288$, 340, and 386 MeV by using the phase shift based on McIntyre parametrization. The calculated elastic cross sections reproduced satisfactorily the diffractive oscillatory structures (at small angles) and refractive patterns (at large angles) observed in the $\alpha + {}^{58}$Ni elastic scatterings. The calculations

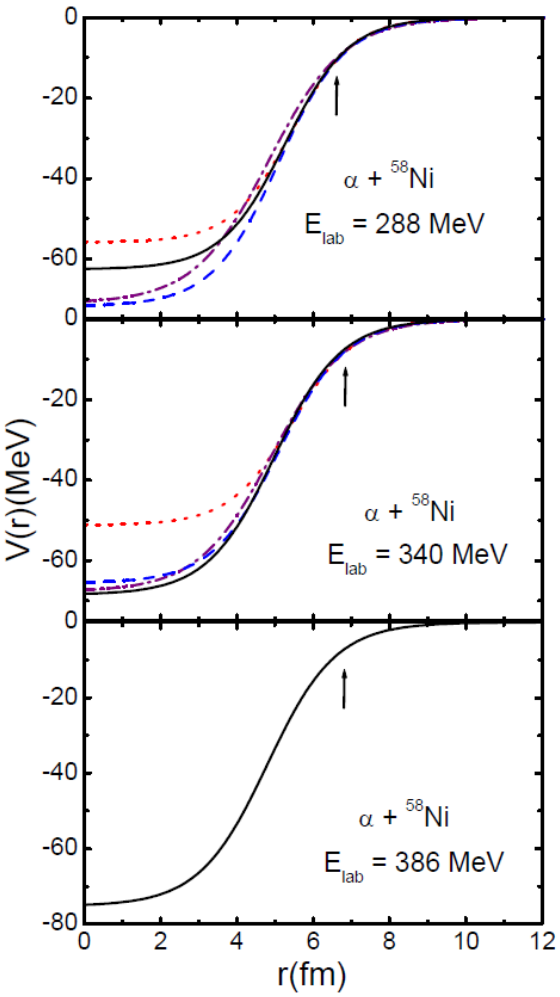

Fig. 3. (Color online) Real parts of optical potential for $\alpha + {}^{58}$Ni elastic scatterings at 288, 340, and 386 MeV, respectively. The dotted, dashed-dotted and dashed curves are the potentials obtained from Set 1, Set 2, and Set 3 listed in Table 2 of Ref. [19]. The solid curves denote the calculated inversion potentials. The arrows indicate the position of the strong absorption radius.

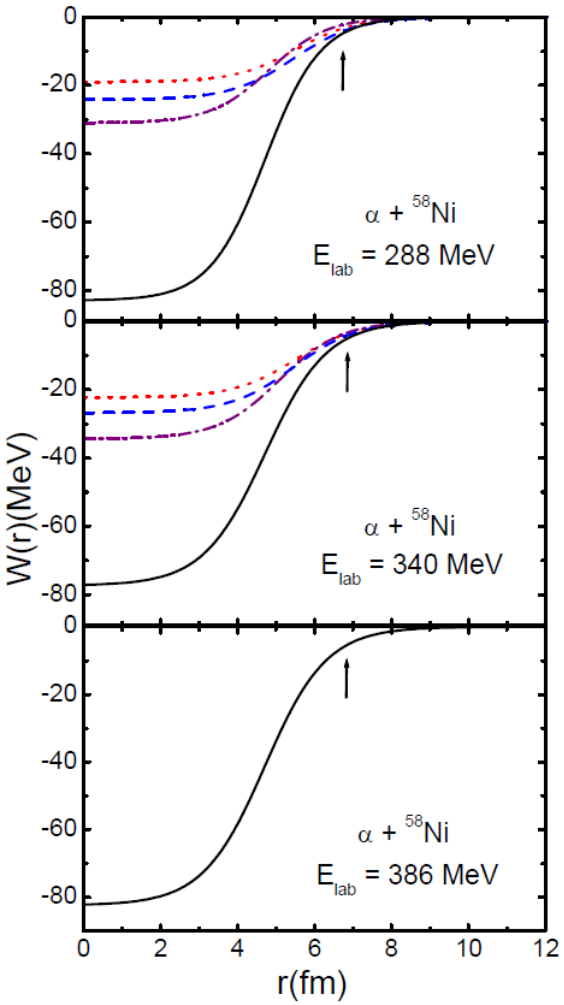

Fig. 4. (Color online) Same as Fig. 3, but for the imaginary parts of optical potential for $\alpha + {}^{58}$Ni elastic scatterings at 288, 340, and 386 MeV, respectively.

were in fairly good agreement with the experimental data over the whole angular and energy ranges. We can see that nuclear rainbow is evidently presented from negative minimum in the deflection functions. The magnitude of reaction cross section could be estimated by strong absorption radius. The near-side and the far-side decompositions of the scattering amplitudes have also been performed by following the Fuller's formalism. The diffractive oscillatory structures observed at small angles have been explained due to the strong interference between the near-side and the far-side scattering amplitudes. However, the structureless exponential fall-off behaviors of the large-angle cross sections are mainly determined by the far-side amplitude.

From the inversion procedure with the relation of McIntyre phase shift and a Woods-Saxon type optical potential, we predicted inversion potentials for $\alpha + {}^{58}$Ni elastic scatterings at 288, 340, and 386 MeV, respectively. As a whole, calculated inversion potentials were found to be in reasonable agreements with the optical model potential in the surface region around the strong absorption radius, but quite different in the interior regions. This implies that the elastic scattering cross sections are mainly sensitive to the surface regions rather than the interior regions. The radial extensions and the radial behaviors of the inversion optical potentials in the surface region are similar to the ones of Woods-Saxon type potential obtained from optical model analysis. We

can further see that the agreements of the real inversion potentials with optical model analysis results are fairly good, in comparison with the ones of the imaginary potentials.

ACKNOWLEDGMENTS

This research was supported by the 2017 scientific promotion program funded by Jeju National University.

REFERENCES

[1] D. M. Brink, *Semi-Classical Methods for Nucleus-Nucleus Scattering* (Cambridge Univ. Press, Cambridge, 1985).
[2] M. C. Mermaz, Z. Phys. A **321**, 613 (1985).
[3] M. C. Mermaz, B. Bonin, M. Buenerd and J. Y. Hostachy, Phys. Rev. C **34**, 1988 (1986).
[4] D. C. Choudhury and M. A. Scura, Phys. Rev. C **47**, 2404 (1993).
[5] S. K. Charagi, S. K. Gupta, M. G. Betigeri, C. V. Fernandes and Kuldeep, Phys. Rev. C **48**, 1152 (1993).
[6] M. H. Cha, J. Korean Phys. Soc. **49**, 1389 (2006).
[7] R. I. Badran, H. Badahdah, M. Arafah and R. Khalidi, Int. J. Mod. Phys. E **19**, 2199 (2010).
[8] J. A. McIntyre, K. H. Wang and L. C. Becker, Phys. Rev. **117**, 1337 (1960).
[9] H. M. Fayyad, T. H. Rihan and A. M. Awin, Phys. Rev. C **53**, 2334 (1996).
[10] N. M. Eldebawi and M. H. Simbel, Phys. Rev. C **53**, 2973 (1996).
[11] I. Ahmad, J. H. Madani and M. A. Abdulmomen, J. Phys. G: Nucl. Part. Phys. **24**, 899 (1998).
[12] Y. J. Kim and M. H. Cha, Int. J. Mod. Phys. E **9**, 299 (2000).
[13] I. Ahmad, M. A. Abdulmomen and G. A. Hamra, Pramana-J. Phys. **65**, 523 (2005).
[14] S. A. Aldenfariya and A. M. Awin, J. Korean Phys. Soc. **64**, 1788 (2014).
[15] M. H. Cha and Y. J. Kim, J. Phys. G: Nucl. Part. Phys. **16**, L281 (1990).
[16] Y. J. Kim and M. H. Cha, Int. J. Mod. Phys. E **8**, 311 (1999).
[17] Y. J. Kim, New Phys.: Sae Mulli **67**, 162 (2017).
[18] K. M. Maung, P. A. Deutchman and W. D. Royalty, Can. J. Phys. **67**, 95 (1989).
[19] B. Bonin, N. Alamanos, B. Berthier, G. Bruce and H. Faraggi *et al.*, Nucl. Phys. A **445**, 381 (1985).
[20] B. K. Nayak, U. Garg, M. Hedden, M. Koss and T. Li *et al.*, Phys. Lett. B **637**, 43 (2006).
[21] R. C. Fuller, Phys. Rev. C **12**, 1561 (1975).